Int. J. Electrochem. Sci., 10 **(2015)** 7465 - 7477

International Journal of
ELECTROCHEMICAL
SCIENCE
www.electrochemsci.org

Comparison of Ca^{2+} Adsorption on (101) and (110) Planes of Rutile Films: A Combined Theoretical and Experimental Investigation

Gang He[1], *Li Xie*[1], *Guang-Fu Yin*[1], *Yuan-Wen Zou*[1,*], *Xiao-Ming Liao*[1], *Zhong-Bing Huang*[1], *Ya-Dong Yao*[1], *Xian-Chun Chen*[1], *Fan-Hou Wang*[2]

[1] College of Materials Science and Engineering, Sichuan University, Chengdu 610064, P. R. China
[2] Computational Physics Key Laboratory of Sichuan Province, Yibin University, Yibin 644000, P. R. China
[*]E-mail: zyw@scu.edu.cn

Received: 5 May 2015 / *Accepted:* 16 June 2015 / *Published:* 28 July 2015

The adsorption of Ca^{2+} on rutile (101) surface and (110) surface was investigated via theoretical and experimental method. The adsorption energy of Ca^{2+} on the bare rutile (101), the bare (110) surfaces, the hydroxylated rutile (101) and the hydroxylated rutile (110) surfaces, were calculated using the Cambridge Sequential Total Energy Package (CASTEP). In order to verify the theoretical results, the immersion experiments in calcium chloride solution with different pH values were carried out. The inductively coupled plasma optical emission spectroscopy (ICP/OES) results demonstrated that in the solution with pH 7.4, there are more Ca^{2+} adsorbed onto R (110) surface than that onto R (101) surface, which should result from the higher Ca^{2+} adsorption ability as shown in the theoretical results. The results of immersion test demonstrate that the pH value has a positive effect on the Ca^{2+} adsorption on (101) or (110) planes of rutile films.

Keywords: Density functional calculations; Adsorption energy; Rutile crystal surfaces

1. INTRODUCTION

In the nature, there are three crystallographic phases of TiO_2, rutile, anatase, and brookite. The rutile form is widely used as a white pigment and opacifier[1] in paints and cosmetics. TiO_2 is also used widely as a catalyst support, and a biocompatible interface for medical implants, or the gas sensors. The chemisorption properties of titanium dioxide are of great interest to both fundamental research and technological applications, particularly in the fields of heterogeneous catalysis, photocatalysis[2-5].

Crystal structure of the titania layer has an important influence on its *in vitro* bioactivity[6], which can be evaluated by examining the apatite formation ability in the simulated body fluid (SBF) [7]. Uchida et al. [8] found that titania particles with amorphous structure did not induce apatite formation on their surfaces, while those with an anatase or rutile structure could induce apatite formation in SBF. They believed that the epitaxy of the apatite crystal could be facilitated by the crystalline planar arrangement in titania crystal structures. The apatite precipitation on three single-crystal rutile substrates: (001), (110), and (100) and a polycrystalline rutile substrate in phosphate buffered saline (PBS) solutions was studied by Lindberg et al.[9], it is found that the speed of hydroxylapatite (HA) deposition on different crystal faces of rutile were different.

Rutile has been extensively studied and widely used in many biomedical applications[10]. The rutile (110) crystal surface (hereafter called R (110)) is the most stable rutile surface, some researches[11, 12] and our previous works[13] indicated that by controlling the electrochemical parameters during the anodic spark oxidation, a high orientation degree of rutile (101) crystal surface (hereafter called R (101)) could be produced, leading to good apatite-forming ability and improving epitaxial growth. As we know, the deposition of calcium ions is the first and most crucial step of the apatite nucleation on ceramic supports from ionic solution, and this process is believed to initiate the growth and formation of bone-like material on the surface of biocompatible implants. Since R (101) may be of importance to good apatite-formatting ability, it is necessary to study the Ca ions adsorption on R (101) surface in detail. Ca ions adsorption on R (110) surface was studied in some papers [14-16], however, there are few published literatures on the specific study of Ca ions adsorption on R (101) surface, besides, there are few published literatures on the comparison of Ca ions adsorption between R (110) and R (101) surface.

In this paper, the Ca ions adsorption on R (110) or R (101) surfaces was investigated, including bare R (110), bare R (101) surface, and both surfaces covered with hydroxyl groups via first-principles calculations based on density functional theory (DFT). To verify the theoretical results and investigate the effect of pH values in the Ca^{2+} adsorption, two types of calcium chloride aqueous solution with different pH values were prepared and immersion experiments were carried out.

2. EXPERIMENTAL AND COMPUTATIONAL DETAILS

2.1. Sample preparation

Rutile titania thin films were prepared via the anodic spark oxidation process, and the detailed procedure was described in our previous study[13]. The degree of rutile (101)-preferred orientation (denoted as γ) was calculated by the ratio of relative diffraction intensities of the rutile (101) to rutile (110) peaks. According to the JCPDS file (no. 21-1276)[17], The γ value of a standard rutile powder is 0.5. Two samples were chosen to compare their experimental differences of Ca ions adsorption: Sample one is named as AOS250 and the γ was 1.48, larger than the γ of standard rutile powder (0.5), indicating that the AOS250 sample has a (101)-preferred orientation. Sample two was named as

AOS2M with γ = 0.67, representing a (110)-preferred orientation. The XRD patterns and SEM micrographs of AOS250 and AOS2M were presented in Fig. 1 and Fig. 2, respectively.

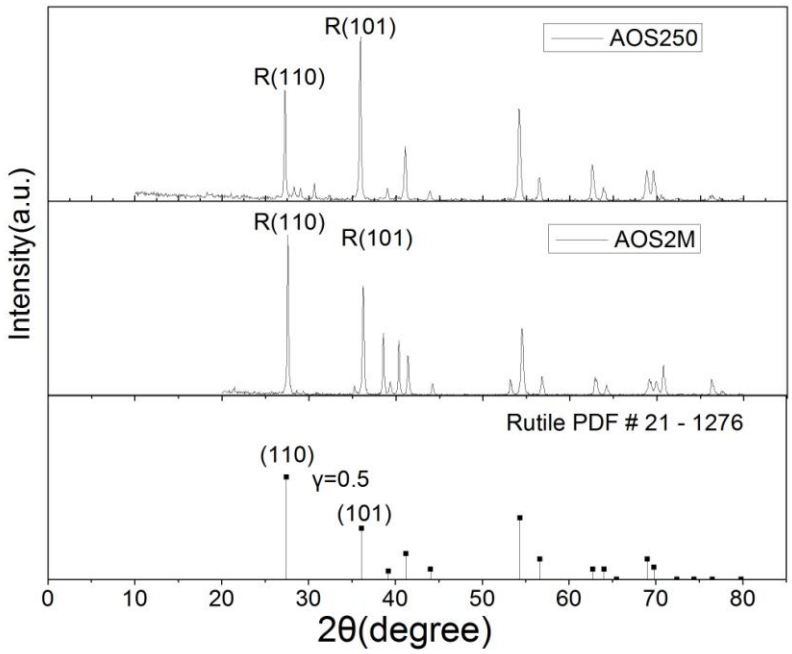

Figure 1. XRD patterns of AOS2M and AOS250

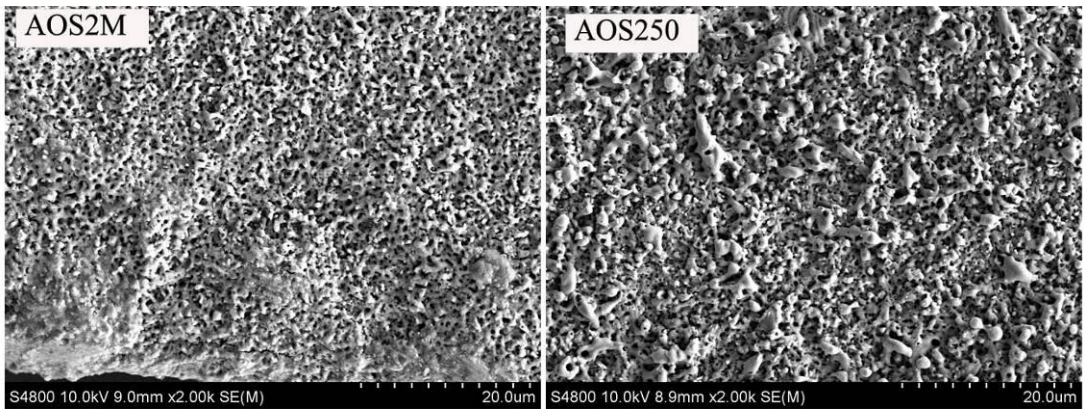

Figure 2. SEM micrographs of AOS2M and AOS250

2.2 Computational details

All geometrical structures were calculated via CASTEP module of Materials Studio software (MS5.5). The generalized gradient approximation (GGA)[6] with spin-polarized Perdew-Wang 1991 (PW91) [10] formulation was used to treat the exchange-correlation function, which has been shown to work well for surfaces[18]. CASTEP calculated the properties of crystals and surfaces by combing pseudopotentials with a plane wave basis [19]. The value of basis set correction[20] dEtot/d log(E_{cut}) can be used to indicate the convergence of the calculations with respect to the value of cut-off energy. According to the results of convergence tests in this study, the value of dEtot/d log(E_{cut}) for the 340 eV

cut-off energy was smaller than 0.1 eV/atom, therefore, this value of E_{cutoff} is sufficient to acheive good convergence for the adsorption energy calculations of Ca on rutile crystal surfaces [8]. The convergence of k-points is achieved with a 4 × 4 × 1 grid[21], as the equilibrium geometry parameters and the value of the total energy showed insignificant variations after increasing the number of k-points from 4 × 4 × 1 to 5 × 5 × 1 or 6 × 6 × 1. Therefore, it can be concluded that this value of k-point was sufficient to calculate the correct energy values for the cases tested in this study[14, 22]. Periodic boundary conditions were used in the bulk and surface slab models. The Ultrasoft Vanderbilt Pseudopotentials (US-PP) with a plane basis set was used to describe the interaction between electrons and ions. In the following calculations, the slab model was used to study the interaction between Ca ion and the R (110) or R (101) surfaces. The 1 × 2 × 2 super cells of R (110) and 1 × 4 × 1 super cells of R (101) were used so as to avoid the interaction of large-size molecules with each other. There were 8 Ti and 14 O atoms existed in the R (110) model and there were 12 Ti and 20 O atoms existed in the R (101) model. These models contained all the typical features of the R (110) and R (101), which has been widely used [23-26]. The surface sizes of R (110) and R (101) are 6.495 Å × 5.866 Å and 6.495 Å × 11.732 Å, respectively. The valence states considered in all the calculations were Ti-$3s_2 3p_6 3d_2 4s_2$, Ca-$3s_2 3p_6 4s_2$, H-$1s_1$and O-$2s_2 2p_4$. The Broyden–Fletcher–Goldfarb–Shanno (BFGS) method was used in order to optimize the structures. The convergence criteria for the Ca^{2+} adsorption energy calculation and geometric optimization of TiO_2 surfaces were set as following: (a) an energy tolerance of 1 × 10^{-5} eV/atom; (b) a self-consistent field tolerance of 1 × 10^{-6} eV/atom; (c) a maximum displacement tolerance of 1.0 × 10^{-3} Å; (d) a maximum force tolerance of 0.03 eV/ Å. Tests on the stability of the structure and the relative energies with the increasing of the accuracy of the parameters were performed, which justified the selection of these parameters. All slab models were separated by a vacuum space of 20.0 Å to avoid the interactions beween the Ca atom and the images of the slab in the neighboring cells, as it is reported that vacuum space larger than 10 Å is enough to avoid the interactions[27]. The atoms in the bottom layer of the rutile crystal surfaces were fixed while the Ca atom and the upper atomic layer of the rutile crystal surfaces were fully relaxed during the optimization process in all of the calculations so as to reduce computational cost[28, 29]. The adsorption energy of the Ca ion on the rutile crystal surface was calculated according to the equation 1:

$$E_{ads} = E_{(Ca+TiO2surface)} - (E_{Ca} + E_{TiO2\ surface}) \quad (1)$$

Where $E_{TiO2\ surface}$ is the energy of the clean TiO_2 surface, E_{Ca} is the energy value of a Ca atom, and $E_{(Ca+TiO2surface)}$ is the total energy of adsorbed Ca on the TiO_2 surface. In this paper, E_{Ca} was calculated by computing the total energy of a large unit cell with a single Ca atom in the middle.

3. RESULTS AND DISCUSSION

3.1 Bulk and surface properties

3.1.1 Bulk properties

To ensure the validity of the computational results, the calculated bulk lattice constants and surfaces energies were compared with data of other literatures. The lattice constants predicted in this

paper are a = 4.593 Å and c = 2.959 Å for rutile, which are in good agreement with the experimental values(a = 4.594 Å and c = 2.958 Å)[9]. The lattice parameters of R (110) and R (101) surface slab used in our computations were compared with those of other published literatures [27], demonstrating that the parameters of our surface slabs of both R (110) and R (101) were accurate and suitable for the Ca^{2+} adsorption calculation.

There are two kinds of titanium atoms[30] existed in the R (110) (Fig. 3a and Fig. 3b). First, a fivefold (5f) pentacoordinated titanium atom, which is under coordinated relative to its bulk structure (noted Ti5f). Second, a sixfold (6f) titanium atom, which is under coordinated relative to the surface bridging oxygen atoms (noted Ti6f). Two kinds of oxygen atoms exhibited in R (110), one is prominent from the surface around 1Å and is only doubly coordinated (noted Ob for "bridging" oxygen), another is localized in the surface plane and is threefold coordinated (noted Os for "surface" oxygen).

The R (101) (Fig. 3c and Fig. 3d) is the third face naturally existed in rutile powder [25]. There are two kinds of atoms existed in R (101) surface. First, a twofold oxygen atom with two different Ti–O bond lengths, noted O(2f); second, a fivefold (5f) pentacoordinated titanium atom, noted Ti(5f).

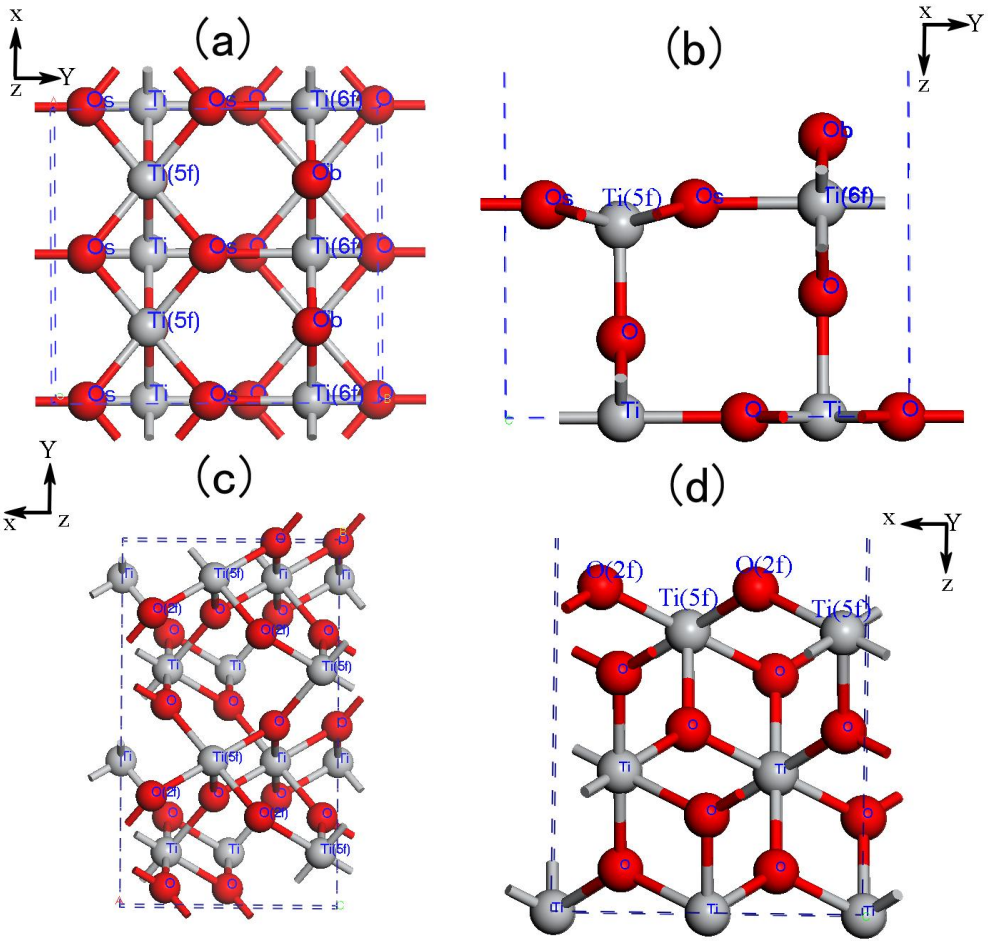

Figure 3. a) Top view of R (110) after geometric optimization. b) Side view of (a). c) Top view of R (101) after geometric optimization. d) Side view of (c). Ca, green; H, white; Ti, grey; O, red. The color code in the following figures remains the same.

3.1.1 Surface properties

The surface energies of our slab models were calculated via equation (2),

$$E_{surf} = (E_{slab} - N \cdot E_{bulk})/(2S) \quad (2)$$

where E_{bulk} is the reference energy for a TiO_2 unit in bulk phase and E_{slab} is the total energy of the supercell, S is the surface area of one side of the slab depending on the considered face and N is the number of TiO_2 units in the supercell. All atomic positions were able to relax during calculations. The surface energy of R (110) was 0.74 J/m^2 and 1.11 J/m^2 for R (101), which were in good agreement with the results calculated from GGA in the literature(0.73[27], 0.81 [31] in J/m^2 for R (110), 1.03[25] in J/m^2 for R (101)).

3.2 The effect of hydroxyl group in the Ca^{2+} adsorption

A large body of literature work [32-36] suggested that there were two features existed in the HA nucleation mechanism. The first feature is that the initial step of the nucleation process is the deposition of Ca^{2+} onto the substrate and then the deposition of phosphate groups with formation of a calcium phosphate phase. The second feature is that the Ca^{2+} deposition is only possible in the presence of hydroxyl groups on the substrate surface[10, 15]. Recently, a series of theoretical and experimental investigations have demonstrated the importance of hydroxyl groups in the nucleation mechanism of apatite[11, 15, 35, 37], and the pretreatments of the surface leading to the binding of hydroxyl groups on the ceramic are effective to induce formation of a stable apatite layer. Therefore, the effect of hydroxyl groups during the Ca^{2+} adsorption process was studied via theoretical and experimental method in this study.

3.2.1 Theoretical study on the effect of hydroxyl groups on the Ca^{2+} adsorption

Two types of R (110) and R (101) surface slab models were presented in this work: the hydroxylated surfaces and the bare surfaces in order to investigate the effect of hydroxyl groups during the adsorption process. The bare R (110) and bare R (101) surface models were presented in Fig. 3, the hydroxylated R (110) and hydroxylated R (101) surface models were given in Fig. 4, the models of Ca^{2+} adsorption on hydroxylated R (110) and hydroxylated R (101) surfaces were presented in Fig. 5. The atoms of hydroxylated surfaces that used in the calculations were presented in Fig. 6. Two optimization processes were executed for Ca^{2+} adsorption on all surface models (bare surfaces and hydroxylated surfaces) .Firstly, an optimization process for the original surface models to obtain an equilibrium state; Secondly, the Ca atoms were added on the pre-optimized surfaces followed by a new optimization process so as to obtain the final equilibrium state. The models shown in Figs. 3, 4, 5 are in equilibrium after geometric optimization. The adsorption energy of Ca^{2+} on different R (110) and R (101) surfaces were presented in Table 1. All values of the adsorption energy calculated in this study were negative as Table 1 presented. The results indicated that all four surfaces can induce Ca adsorption and the ability of rutile surfaces to induce Ca adsorption, including the bare rutile surfaces

(surfaces without any modification), is consistent with previous reports[38, 39]. It is obvious that the absolute values of adsorption energy of Ca^{2+} on bare R (110) or hydroxylated R (110) were higher than that on bare R (101) or hydroxylated R (101) respectively, which means the adsorbed structures of Ca^{2+} on bare R (110) or hydroxylated R (110) are more stable than that of Ca^{2+} on bare R (101) or hydroxylated R (101).

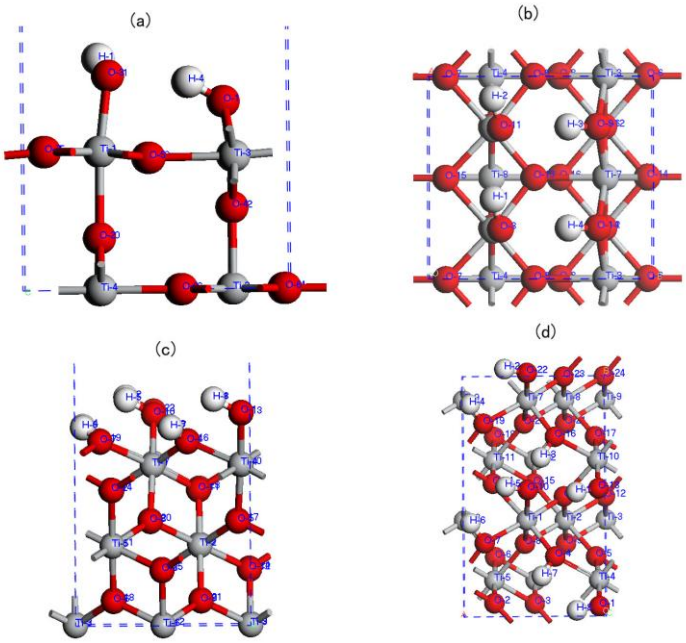

Figure 4. a) Side view of the hydroxylated R (110) after geometric optimization. b) Top view of (a). c) Side view of the hydroxylated R (101) surface after geometric optimization. d) Top view of (c).

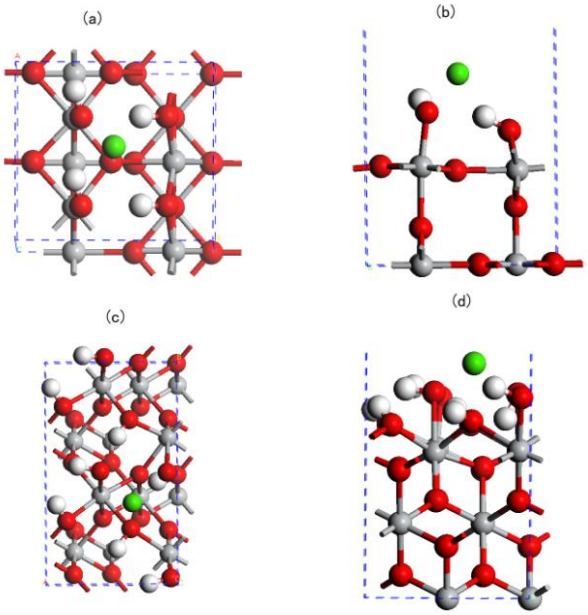

Figure 5. a) Top view of Ca^{2+} adsorption model on hydroxylated R (110) surface. b) Side view of (a). c) Top view of Ca^{2+} adsorption model on hydroxylated R (101) surface. d) Side view of (c).

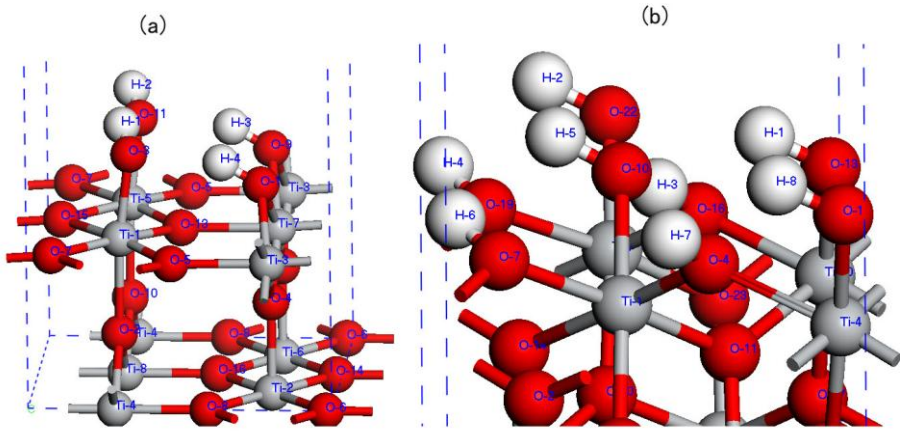

Figure 6. a) The labels of the atoms used in the calculation for hydroxylated R (110) surface. b) The labels of the atoms used in the calculation for hydroxylated R (101) surface.

Table 1. Adsorption energy between different R (110) and R (101) surfaces and the Ca atom (unit:eV)

Substrates	$E_{(Ca+TiO2Surface)}$	$E_{TiO2surface}$	E_{Ca}	E_{ads}
Bare R(110)	-19970.71	-18967.66	-999.52	-3.53
Bare R(101)	-29010.84	-28008.11	-999.52	-3.21
Hydroxylated R(110)	-13404.65	-12401.52	-999.52	-3.62
Hydroxylated R(101)	-20964.65	-19961.79	-999.52	-3.33

The analyses of the electronic density of state (DOS) were carried out so as to investigate the bonding details of the adsorbed Ca^{2+} on hydroxylated R (110) and hydroxylated R (101) surfaces.

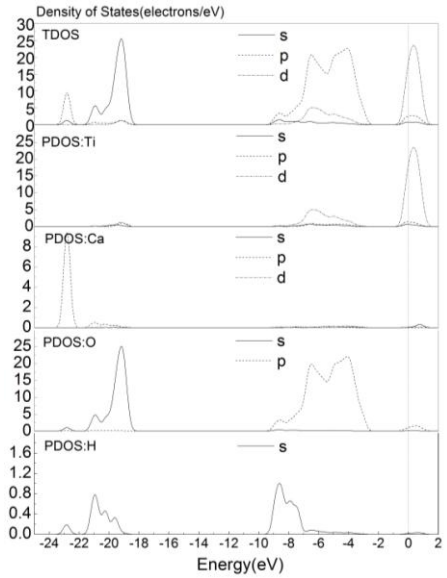

Figure 7. DOS(TDOS， PDOS) of the Ca^{2+} adsorption on hydroxylated R (110) surface.

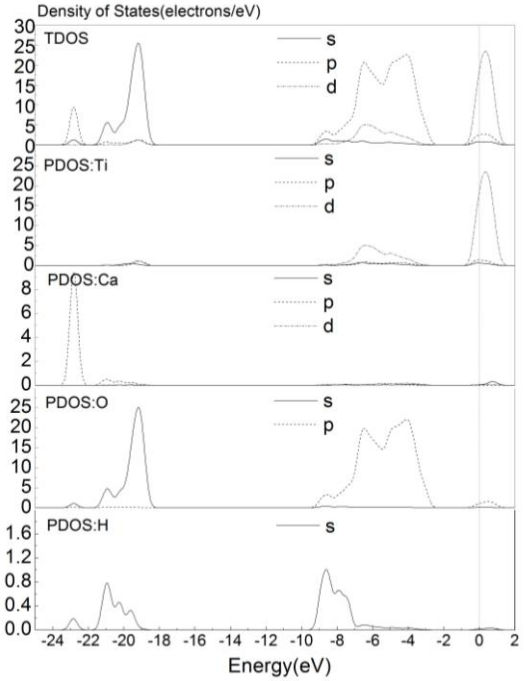

Figure 8. DOS(TDOS， PDOS) of the Ca^{2+} adsorption on hydroxylated R (101) surface.

The partial density of states (PDOS) and the total density of state (TDOS) of Ca^{2+} adsorption on hydroxylated R (110) and R (101) were presented in Fig. 7 and Fig. 8. The TDOS and PDOS of all the atoms of R (110) and R (101) have similar shapes. In both situations, the antibonding states above the Fermi level mainly comes from Ca4s and Ti3d and partially from H1s in the energy range of 0–2 eV. There are overlapping peaks existed between the PDOS of the Ca2p and O2s, as well as the PDOS of the Ca3d and O2p. There may be substantial hybridization existed between the Ca3d and O2p[14]. The DOS results of both situations demonstrated that the main bonding occurs between Ca and O.

In order to demostrate the electron transfers and interactions among different atoms during Ca^{2+} adsorption on R (110) and R (101) surfaces, the population analysis was performed using a projection of the plane wave states onto a localized basis set. The Mulliken formalism[40] was used to analyze the projected states. The overlapping populations between the Ca atoms and O atoms on both hydroxylated R (110) and hydroxylated R (101) surfaces were presented in Table 2. A large positive value indicates a bonding state between the Ca and O atoms; a large negative value indicates an antibonded state between them; a value close to zero indicates that there is no significant interaction between the electron populations of the Ca and O atoms[41]. In the case of Ca^{2+} adsorption on hydroxylated R (110) surface, the values of overlapping populations between Ca and O3 or O11 were found to be relatively high (two bonds with the same population of 0.18), indicating a weakly covalence in the bonds between O3–Ca and O11–Ca. On the other hand, the overlapping populations between Ca and H were found to be -0.01 ~ -0.03, indicating that they were in an antibonded state. In the case of hydroxylated R (101) surfaces, there were strong bonds between the O and Ca atoms too. The overlapping population between O10 or O13 and Ca were 0.16 and 0.14, respectively, There also existed antibonding interactions between H and Ca with the value of overlapping population in the

range of -0.01 ~ -0.04. The detailed population results were presented in table 2. The results demonstrate that the bond between O and Ca is the main factor of Ca^{2+} adsorption, it also reveals that there are stronger Ca-O bond on hydroxylated R (110) surface (two bonds with the same population of 0.18) than that on hydroxylated R (101) surface (one bond with population of 0.16 and the other of 0.14).

Table 2. The bond population and the distances of atoms on the hydroxylated R(110) and R(101) after Ca^{2+} adsorption

Surface	Bond	bond population	Distance(Å)
$R(110)_{OH}$	O 11 -- Ca	0.18	2.17
$R(110)_{OH}$	O 3 -- Ca	0.18	2.20
$R(110)_{OH}$	O 1 -- Ca	0.07	2.37
$R(110)_{OH}$	O 9 -- Ca	0.04	2.46
$R(110)_{OH}$	O 13 -- Ca	0.04	2.39
$R(110)_{OH}$	H 1 -- Ca	-0.03	2.85
$R(101)_{OH}$	O 10 -- Ca	0.16	2.13
$R(101)_{OH}$	O 13 -- Ca	0.14	2.20
$R(101)_{OH}$	O 4 -- Ca	0.09	2.22
$R(101)_{OH}$	H 1 -- Ca	-0.02	2.31

3.2.2 Experimental study on the effect of hydroxyl groups on the Ca^{2+} adsorption

The hydroxyl groups play a crucial role in the adsorption of calcium, and the following apatite nucleation. In this study, ICP/OES method is used to analyze the changes of Ca^{2+} concentration during the adsorption process. The pH value of the $CaCl_2$ aqueous solution was measured by a PHS-3C pH meter (Rex Instrument Factory, Shanghai, China). All samples were immersed in calcium chloride aqueous solution at 37ºC in a shaking bath. In Order to investigate the effect of hydroxyl group on the Ca^{2+} adsorption, calcium chloride aqueous solution with the same Ca^{2+} concentration and pH value as blood plasma (2.5×10^{-3} mol/L for Ca^{2+} concentration[42], pH about 7.4[43, 44]) was used in the immersion test. The Ca^{2+} concentration values of the calcium chloride aqueous solution during the immersion were presented in Fig. 9 (dashed lines with pH 7.4). After 6 hours of immersion, the Ca^{2+} concentration of the solution with AOS2M was slightly lower than that with AOS250; After 12 hours and 24 hours immersion, it can be clearly observed that the Ca^{2+} concentration of the solution with AOS2M was lower than that with AOS250; demonstrating that the AOS2M sample has stronger Ca^{2+} adsorption ability than that of AOS250, and (110) orientated sample has better Ca^{2+} adsorption ability than that of (101) orientated sample.

3.3 The effect of pH values in the Ca^{2+} adsorption

It is reported that the adsorption of Ca^{2+} should be favored by raising the pH value of the solution[15] because of the increase of the hydroxyl groups in the solution. To investigate the effect of

pH values in the Ca^{2+} adsorption, two types of calcium chloride aqueous solution with different pH values were prepared. Both types of solution had the same Ca^{2+} concentration as blood plasma as reported in the literatures[45]. Solution one was prepared by dissolving calcium chloride in double distillated water and pH value was about 5.6. Solution two was prepared by dissolving calcium chloride in double distillated water and then $Ca(OH)_2$ solution was used to raise the pH of the solution to about 7.4. The Ca^{2+} concentration values of both types of solution during the immersion test were presented in Fig. 9. It can be observed that in the solution of pH 5.6, the Ca^{2+} concentration of the solution with AOS2M is lower than that with AOS250 after 6 h, 12 h and 24 h immersion. Moreover, there was obviously more Ca^{2+} existed in solution one (with pH about 5.6) compared with that in solution two (with pH about 7.4) after 6 h, 12 h and 24 h immersion, confirming that raising the pH value of the solution is favor of the adsorption of Ca^{2+} on both (110) and (101) planes of rutile films.

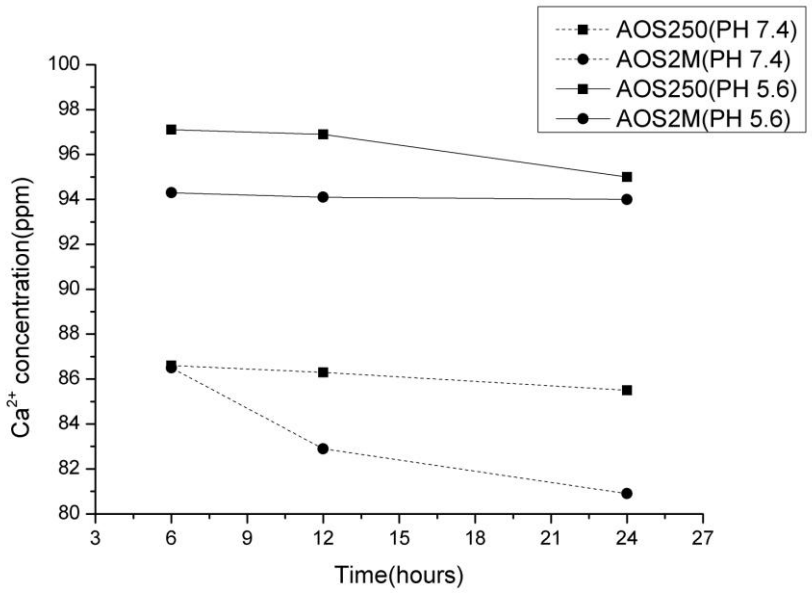

Figure 9. Ca^{2+} concentration of the $CaCl_2$ aqueous solution during the immersion.

4. CONCLUSIONS

Theoretical calculations demonstrate that the calcium ions adsorption ability on hydroxylated R (101) and hydroxylated R (110) surfaces are different from on bare R (101) and R (110) surfaces: the adsorption ability of calcium ions on hydroxylated R (110) surface is stronger than hydroxylated R (101) surface because of stronger Ca-O bond, which may result from the existence of hydroxyl groups. Experimental results demonstrate that in the calcium chloride aqueous solution with pH 7.4, there were more Ca ions adsorbed onto R (110) surface than that of R (101) surface after 6 h, 12 h and 24 h immersion. The pH value has a positive effect on the Ca^{2+} adsorption in chloride aqueous solution. These experimental and theoretical results determine that with the existence of hydroxyl groups, R

(110) surface demonstrates better Ca^{2+} adsorption ability than that of R (101) surface, which might accelerate the HA deposition speed on rutile titanium dioxide substrate.

ACKNOWLEDGEMENTS
This work has been supported by the National Natural Science Foundation of China (project No. 51273122 and 51173120).

References

1. J. Muscat, V. Swamy, N. M. Harrison, *Phys. Rev. B*, 65 (2002)224112.
2. M. A. Fox, M. T. Dulay, *Chemical Reviews*, 93 (1993)341.
3. N. Serpone, E. Pelizzetti, *Photocatalysis : fundamentals and applications*. (Wiley, New York [etc.], 1989).
4. V. E. Henrich, P. A. Cox, *The surface science of metal oxides*. (Cambridge university press, 1996).
5. A. L. Linsebigler, G. Lu, J. T. Yates, *Chem. Rev.*, 95 (1995)735.
6. J. P. Perdew, K. Burke, M. Ernzerhof, *Phys. Rev. Lett.*, 77 (1996)3865.
7. T. Kokubo, H. Takadama, *Biomaterials*, 27 (2006)2907.
8. D. Vanderbilt, *Phys. Rev. B*, 41 (1990)7892.
9. F. Lindberg, J. Heinrichs, F. Ericson, P. Thomsen, H. Engqvist, *Biomaterials*, 29 (2008)3317.
10. J. P. Perdew, Y. Wang, *Phys. Rev. B*, 45 (1992)13244.
11. B. Yang, M. Uchida, H.-M. Kim, X. Zhang, T. Kokubo, *Biomaterials*, 25 (2004)1003.
12. X. Cui, H. M. Kim, M. Kawashita, L. Wang, T. Xiong, T. Kokubo, T. Nakamura, *Dental Materials*, 25 (2009)80.
13. G. He, L. Xie, G.-F. Yin, X.-M. Liao, Y.-W. Zou, Z.-B. Huang, Y.-D. Yao, X.-C. Chen, F.-H. Wang, *Surf. Coat. Technol.*, 228 (2013)201.
14. X. Lu, H.-p. Zhang, Y. Leng, L. Fang, S. Qu, B. Feng, J. Weng, N. Huang, *J. Mater. Sci. Mater. Med.*, 21 (2010)1.
15. M. Svetina, L. Colombi Ciacchi, O. Sbaizero, S. Meriani, A. De Vita, *Acta Materialia*, 49 (2001)2169.
16. M. A. San Miguel, J. Oviedo, J. F. Sanz, *The Journal of Physical Chemistry C*, 113 (2009)3740.
17. I. C. f. D. D. JCPDS Card No. 21-1276 (Joint Committee on Powder Diffraction Standards, Swarthmore, PA, Rutile TiO2), 1996.
18. C. Y. Chang, H.-T. Chen, M. Lin, *The Journal of Physical Chemistry C*, 113 (2009)6140.
19. S. J. Clark, M. D. Segall, C. J. Pickard, P. J. Hasnip, M. I. Probert, K. Refson, M. C. Payne, *Zeitschrift für Kristallographie*, 220 (2005)567.
20. G. Francis, M. Payne, *J. Phys.: Condens. Matter*, 2 (1990)4395.
21. H. J. Monkhorst, J. D. Pack, *Phys. Rev. B*, 13 (1976)5188.
22. Z. Zhang, P. Fenter, S. D. Kelly, J. G. Catalano, A. V. Bandura, J. D. Kubicki, J. O. Sofo, D. J. Wesolowski, M. L. Machesky, N. C. Sturchio, *Geochim. Cosmochim. Acta*, 70 (2006)4039.
23. S. Bates, G. Kresse, M. Gillan, *Surf. Sci.*, 409 (1998)336.
24. W. Langel, *Surf. Sci.*, 496 (2002)141.
25. H. Perron, C. Domain, J. Roques, R. Drot, E. Simoni, H. Catalette, *Theor. Chem. Acc.*, 117 (2007)565.
26. B. J. Morgan, G. W. Watson, *The Journal of Physical Chemistry C*, 113 (2009)7322.
27. S. Bates, G. Kresse, M. Gillan, *Surf. Sci.*, 385 (1997)386.
28. Y. Han, C.-j. Liu, Q. Ge, *The Journal of Physical Chemistry B*, 110 (2006)7463.

29. N. Lopez, J. K. Nørskov, *J. Am. Chem. Soc.*, 124 (2002)11262.
30. U. Diebold, *Surf. Sci. Rep.*, 48 (2003)53.
31. P. Lindan, N. Harrison, M. Gillan, J. White, *Phys. Rev. B*, 55 (1997)15919.
32. H. Takadama, H. M. Kim, F. Miyaji, T. Kokubo, T. Nakamura, *J. Ceram. Soc. Jpn.*, 108 (2000)118.
33. H. Takadama, H. M. Kim, T. Kokubo, T. Nakamura, *J. Biomed. Mater. Res.*, 57 (2001)441.
34. H. Takadama, H.-M. Kim, F. Miyaji, T. Kokubo, T. Nakumura, in *BIOCERAMICS-CONFERENCE-*. (vol. 11, 1998 pp. 663-666.
35. T. Kokubo, *Acta Mater.*, 46 (1998)2519.
36. B. Yang, J. Weng, X. Li, X. Zhang, *J. Biomed. Mater. Res.*, 47 (1999)213.
37. T. Miyazaki, H.-M. Kim, T. Kokubo, C. Ohtsuki, H. Kato, T. Nakamura, *Biomaterials*, 23 (2002)827.
38. R. Rohanizadeh, M. Al‐Sadeq, R. LeGeros, *Journal of Biomedical Materials Research Part A*, 71 (2004)343.
39. X.-X. Wang, W. Yan, S. Hayakawa, K. Tsuru, A. Osaka, *Biomaterials*, 24 (2003)4631.
40. R. S. Mulliken, *The Journal of Chemical Physics*, 23 (2004)1833.
41. M. Segall, R. Shah, C. Pickard, M. Payne, *Phys. Rev. B*, 54 (1996)16317.
42. J. L. Gamble, *Chemical anatomy, physiology and pathology of extracellular fluid: a lecture syllabus*. (Harvard University Press, 1947).
43. M. Bohner, J. Lemaitre, *Biomaterials*, 30 (2009)2175.
44. T. Rosenthal, *J. Biol. Chem.*, 173 (1948)25.
45. E. N. Marieb, K. Hoehn, *Human anatomy & physiology*. (Pearson Education, 2007).